# Compound nuclear reaction mechanisms of light composite particles

*Brett V.* Carlson[1,*], *Roberto* Capote[2], *Mihaela* Sin[3], and *Fatemeh* Torabi[4]

[1]Departamento de Física, Instituto Tecnológico de Aeronáutica, 12228-900 São José dos Campos SP, Brazil
[2]Nuclear Data Section, Division of Physical and Chemical Sciences, Department of Nuclear Sciences and Applications, International Atomic Energy Agency, POB 100, Vienna, Austria
[3]Faculty of Physics, University of Bucharest, P.O. Box MG-11, 70709 Bucharest-Magurele, Romania
[4]Departamento de Ciencias Integradas, Facultad de Ciencias Experimentales, Universidad de Huelva, 21071 Huelva, Spain

**Abstract.** We assess the ability of a light-composite breakup model coupled to pre-compound and compound statistical emission models to describe selected compound nuclear cross sections. The framework employed calculates elastic and nonelastic breakup differential cross sections using the post-form distorted wave Born expressions of the Ichimura-Austern-Vincent approach. This has been incorporated into the EMPIRE nuclear reaction code for the specific case of the deuteron, used in the calculations presented here. The exciton pre-equilibrium and Hauser-Feshbach compound-nucleus models are used to account for pre-equilibrium and equilibrium emission. The outcome of our analyses yields a satisfactory agreement between theoretical and experimental values in most cases. The analysis also permits a preliminary assessment of the importance of inelastic excitation on the cross-section predictions.

## 1 Introduction

Many light composite nuclei, such as the deuteron, $^{6}$He and $^{6,7}$Li and, to a lesser extent, the triton and $^{3}$He, are weakly-bound and thus fragment easily in a nuclear reaction. Methods to describe such reactions, such as the post-form distorted-wave Born expression (DWBA) of the Ichimura-Austern-Vincent (IAV) approach [1–4] and the continuum-discretized coupled channels (CDCC) method [3], were developed several decades ago, but have become more visible in recent years [5–8], with the increase in computing power to perform calculations and of experimental data to analyze. Although limited to single-step reactions, the IAV approach has an advantage over the more powerful CDCC method in that it can also calculate the contribution of nonelastic breakup, in which one of the fragments fuses with the target. The sum of both contributions is necessary to estimate inclusive cross sections in the region of the breakup peak.

Other reactions, such as pre-equilibrium and equilibrium compound nuclear emission also make small contributions to inclusive particle emission in the region of the breakup peak. Outside this region, their contributions can be the most important ones. The breakup reaction also affects compound nuclear emission cross sections by reducing the contribution of projectile + target fusion but including those of fragment + target fusion. In the simplest case of two-body breakup, the compound nuclear problem must contend with three initial configurations: fusion of the projectile and target as well as fusion of each of the fragments with the target, which can occur over the wide range of energies resulting from the breakup. These modifications make small changes in the inclusive emission spectra, but are essential to the description of more specific compound nucleus reactions.

In the following, we will discuss the simple case of deuteron breakup. As the deuteron is weakly bound, its breakup cross section is large and the modifications to compound nuclear cross sections due to its breakup are also relatively large. This case also has the advantage that the two fragments, a proton and a neutron, are inert particles with no excited states on the scale of low-energy nuclear physics. The formalism thus need only take into account their kinetic energies.

The EMPIRE [9] code stands out as an extremely versatile tool for nuclear-reaction analyses, being capable of estimating production cross sections of residual nuclei after multiple particle emission, as well as the spectra and angular distributions of emitted particles. This code has been modified to include the IAV approach [1–4] for deuteron breakup. This enables the code to take into account elastic deuteron breakup, in which both the proton and neutron emerge, leaving the target in its ground state, as well as the nonelastic breakup, in which one nucleon is absorbed or transferred while the other is emitted. The modified code has already been utilized in our earlier investigation [8] of various sets of double differential experimental data for deuteron-induced inclusive (d,xn) and (d,xp) emission. The present work focuses on evaluating the ability of this updated version of EMPIRE to predict compound nucleus cross sections, in particular, total (d,2n) production cross sections, over a wide range of energies, as well as the exclusive (d,pf) cross section.

*e-mail: brett@ita.br

## 2 Formalism

We use the zero-range post-form IAV formalism to calculate the elastic (EBU) and nonelastic (NEB) breakup [1–4] and compound nucleus formation cross sections, coupled to the EMPIRE nuclear reaction code [5], to calculate compound nucleus emission cross sections. The breakup process is a direct reaction that produces protons and neutrons with a wide range of energies and angular momenta. The inclusive proton breakup emission cross section can be decomposed into a part in which both the proton and neutron are emitted and a part in which the proton is emitted but the neutron is absorbed. We assume that the target acts as a spectator to the breakup and denote the contribution in which both proton and neutron are emitted as elastic breakup (EBU). We label the remaining contribution as nonelastic breakup (NEB, p) and assume that it corresponds solely to breakup followed by emission of the proton and absorption of the neutron by the target. We have

$$\frac{d^2\sigma}{d\Omega_p dE_p} = \frac{d^2\sigma^{EBU}}{d\Omega_p dE_p} + \frac{d^2\sigma^{NEB,p}}{d\Omega_p dE_p} . \quad (1)$$

The contribution of the elastic breakup is written in terms of its T-matrix element as

$$\frac{d^2\sigma^{EBU}}{d\Omega_p dE_p} = \frac{2\pi}{\hbar v_d}\rho_p(E_p)\int |T(\vec{k}_p,\vec{k}_n;\vec{k}_d)|^2 \times\delta(E_d+\varepsilon_d-E_p-E_n)\,d\vec{k}_n , \quad (2)$$

with the final momentum density $\rho_p(E_p) = \frac{\mu_p k_p}{8\pi^3\hbar^2}$, and $\vec{k}_d$, $\vec{k}_n$, and $\vec{k}_p$ representing the initial deuteron momentum, and the final neutron and proton momenta, respectively. The $\delta$-function constrains the sum of the neutron and proton final kinetic energies to that of the initial deuteron kinetic energy and its binding energy.

The T-matrix element is approximated by the post-form of the DWBA matrix element as

$$T\left(\vec{k}_p,\vec{k}_n;\vec{k}_d\right) = \int d^3r_{pn}\,d^3r_{dA}\,\chi^{(-)\dagger}_{\vec{k}_p}\left(\vec{r}_{pB}\right)\chi^{(-)\dagger}_{\vec{k}_n}\left(\vec{r}_{nA}\right) \times V\left(\vec{r}_{pn}\right)\phi_d\left(\vec{r}_{pn}\right)\chi^{(+)}_{\vec{k}_d}\left(\vec{r}_{dA}\right) , \quad (3)$$

where $B = A + 1$, $A$ being the target mass, and $V\left(\vec{r}_{pn}\right)$ the proton-neutron interaction. Using the local energy approximation of Buttle and Goldfarb [10] and Benzce and Zimanyi [11], the DWBA matrix element can be rewritten as

$$T\left(\vec{k}_p,\vec{k}_n;\vec{k}_d\right) = D_0\int d^3r\,\Lambda\left(\vec{r}\right)\chi^{(-)\dagger}_{\vec{k}_p}\left(\alpha\vec{r}\right)\chi^{(-)\dagger}_{\vec{k}_n}\left(\vec{r}\right)\chi^{(+)}_{\vec{k}_d}\left(\vec{r}\right) , \quad (4)$$

where $D_0$ is given by

$$D_0 = \int dr^3_{pn}\,V\left(\vec{r}_{pn}\right)\phi_d\left(\vec{r}_{pn}\right) \approx 125\ \text{MeV-fm}^{3/2} . \quad (5)$$

and $\Lambda\left(\vec{r}\right)$ is the finite-range correction factor. Although originally derived as an approximation to the matrix elements of stripping to bound states, we have found this approximation to be equally applicable to stripping reactions to the continuum, that is, to breakup reactions.

The nonelastic breakup cross section is given by an expectation value of the imaginary part of the optical potential between the absorbed particle and the target as,

$$\frac{d^2\sigma^{NEB,p}}{d\Omega_p dE_p} = -\frac{2}{\hbar v_d}\rho_p(E_p)\left\langle\Psi_n(\vec{k}_p,\vec{r};\vec{k}_d)\right| \times W_{nA}\left(\vec{r}\right)\left|\Psi_n(\vec{k}_p,\vec{r};\vec{k}_d)\right\rangle , \quad (6)$$

where the effective neutron wave function, in the zero-range approximation, is given by

$$\left|\Psi_n\left(\vec{k}_p,\vec{r};\vec{k}_d\right)\right\rangle = D_0\int d^3r'\,\Lambda\left(\vec{r}'\right)\chi^{(-)\dagger}_{\vec{k}_p}\left(\alpha\vec{r}'\right) \times G^{(+)}_n\left(\vec{r},\vec{r}'\right)\chi^{(+)}_{\vec{k}_d}\left(\vec{r}'\right) . \quad (7)$$

The inclusive double differential proton breakup cross section is the sum of the elastic and nonelastic breakup cross sections given above. We do not take into account the contribution of inelastic excitation before or after breakup. The inclusive neutron breakup cross section is obtained by exchanging the proton and neutron labels in the expressions above.

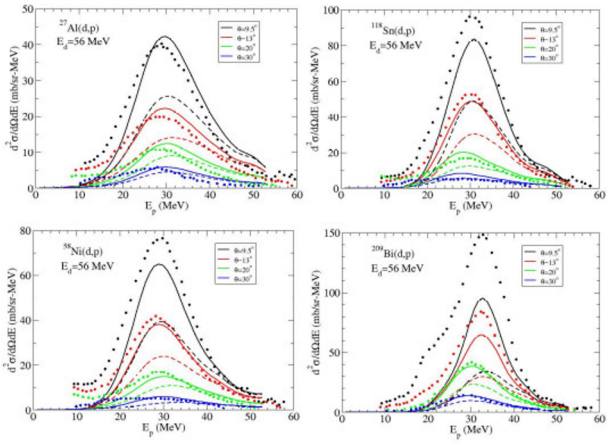


**Figure 1.** Inclusive double differential proton spectra at several angles from deuterons incident on the target nuclei $^{27}$Al, $^{58}$Ni, $^{118}$Sn, and $^{209}$Bi at 56 MeV are compared to the experimental data of Ref. [18]

The double differential cross sections are calculated by reducing the expressions above to partial wave sums over the orbital angular momenta of the proton $l_p$, neutron $l_n$ and deuteron $l_d$. Spin-orbit effects are neglected. The correct energy-dependent optical potentials are used for each partition of the energy between the proton and the neutron. Efficient convergence of the radial integrals is obtained by using the complex-plane integration method of Vincent and Fortune [12]. Angular momentum convergence of the double differential elastic cross section has been confirmed by comparison with the analytical expression for the Coulomb breakup cross section [13–15]. The

optical potentials used for the neutron and proton were the global potentials of Koning-Delaroche [16], while the global potential of An-Cai [17] was used for the deuteron. More information concerning the numerical details of the elastic and nonelastic breakup calculations can be found in Ref [6].

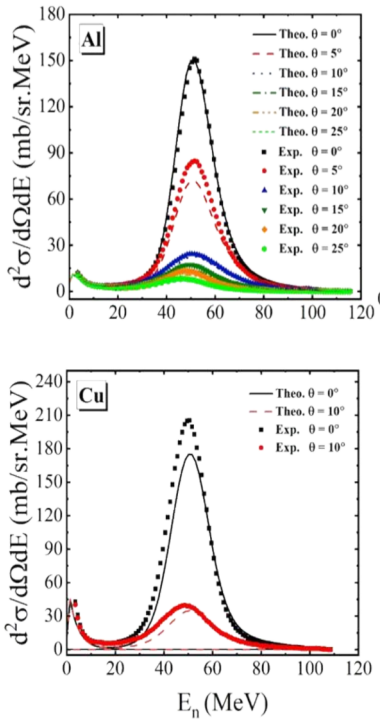


**Figure 2.** Inclusive double differential neutron spectra at several angles from deuterons incident on the target nuclei Al and Cu at 102 MeV are compared to the experimental data of Ref.[19]

In Fig. 1, we compare differential proton spectra in the region of the elastic breakup peak with experimental data for deuterons incident on $^{27}$Al, $^{58}$Ni, $^{118}$Sn, and $^{209}$Bi targets at 56 MeV [18]. The differential cross sections are forward peaked and fall off rapidly with angle. The calculated distributions agree fairly well with the data for light nuclei but underestimate the most forward angle data by an increasing amount as the target mass and charge increase. A systematic shift of the experimental spectra to lower energies suggests that inelastic excitation of the target could play an increasingly important role as the target mass and charge increase. In Fig.2, we compare differential neutron spectra in the region of the elastic breakup peak with experimental data for deuterons incident on Al and Cu targets at 102 MeV [19]. As in the case of protons, the differential neutron distributions are forward peaked and show good agreement with the experimental data, but with increasing discrepancies at the most forward angles as the mass and charge of the target increase. All in all, we find that the model provides a reasonably good description of the inclusive nucleon differential spectra.

In order to analyze experimental data for inclusive particle emission, we have taken into account the contributions of other processes to the emission. We assume the most important of these to be pre-equilibrium and equilibrium emission from the compound nucleus. To describe these emission mode, we use the phenomenological exciton model and the statistical Hauser-Feshbach emission model, respectively. Our calculations were made using a modified version of the code EMPIRE [9]. In the inclusive nucleon emission spectra, the pre-compound and compound contributions to the differential spectra are most important at low and high emission energies, outside the breakup peak. For the compound nucleus cross sections we will discuss in the following, these contributions are essential.

Three different pre-compound/compound nuclei are formed in a deuteron breakup reaction, those in which the neutron or proton is absorbed by the target and that in which the initial deuteron is absorbed. As the breakup of the deuteron results in protons and neutrons with a wide range of energies, the compound nuclei formed by their absorption possess a wide range of excitation energies. The differential cross sections for neutron and proton absorption are obtained from the partial wave decomposition of the nonelastic absorption cross sections. Neglecting spin-orbit coupling, for simplicity, this decomposition furnishes a partial wave differential cross section dependent on the orbital angular momenta of the neutron, proton, and deuteron that, when summed over the angular momenta of the deuteron and the emitted particle, provides the contribution to the differential cross section due to nonelastic breakup, $d\sigma_{l_p}^{NEB,p}/dE_p$ or $d\sigma_{l_n}^{NEB,n}/dE_n$. These contributions are integrated into the correct residual nucleus distribution of the pre-compound decay chain in the EMPIRE code. For example, the differential cross section $\left(d\sigma_{l_p}^{NEB,p}/dE_p\right)\Delta E_p$ at an energy $E_p$ is summed with the population of the residual nucleus $(Z_T+1, A_T+1)$ at excitation energy $E^* = E_p + S_p$ and angular momentum $l_p$, where $S_p$ is the separation energy of the proton from the target $(Z_T, A_T)$ and $\Delta E_p$ is the energy bin of the statistical decay calculation. (This residual population also contains a contribution due to neutron emission from the nucleus $(Z_T+1, A_T+2)$ formed by the fusion of the deuteron with the target.) The nonelastic breakup thus yields a continuum of pre-compound nuclei that must be considered together with the residual distribution resulting from single proton/neutron emission after fusion of the deuteron and the target. The reaction code EMPIRE was modified to integrate these contributions into the decay chain automatically.

The partial wave cross sections obtained from the deuteron optical potential calculation, $\sigma_{l_d}^{reac}$ , describe the partial wave contributions to the reaction cross section and thus implicitly take into account the effects of the elastic and nonelastic breakup. The latter must be subtracted to obtain the effective partial cross sections for deuteron absorption, $\sigma_{l_d}^{d}$. We thus have

$$\sigma_{l_d}^{d} = \sigma_{l_d}^{reac} - \sigma_{l_d}^{NEB,p} - \sigma_{l_d}^{NEB,n} - \sigma_{l_d}^{EBU} , \qquad (8)$$

where the partial differential elastic and nonelastic breakup cross sections are now summed over the proton

and neutron angular momenta indices, leaving only the deuteron angular momentum index, which we write as

$$\frac{d\sigma_{l_d}^{NEB,p}}{dE_p}, \quad \frac{d\sigma_{l_d}^{NEB,n}}{dE_n} \text{ and } \frac{d\sigma_{l_d}^{EBU}}{dE_p},$$

and then integrated over energy to obtain the partial absorption cross sections,

$$\begin{aligned} \sigma_{l_d}^{NEB,p} &= \int \frac{d\sigma_{l_d}^{NEB,p}}{dE_p} dE_p \\ \sigma_{l_d}^{NEB,n} &= \int \frac{d\sigma_{l_d}^{NEB,n}}{dE_n} dE_n \\ \sigma_{l_d}^{EBU} &= \int \frac{d\sigma_{l_d}^{EBU}}{dE_p} dE_p \,. \end{aligned} \tag{9}$$

We have written the elastic breakup cross section as a function of the proton energy $E_p$, although it can be written equally well in terms of the elastic breakup neutron energy $E_n = E_d - B_d - E_p$.

The deuteron absorption cross section $\sigma_{l_d}^{d}$ can become negative at large values of the angular momentum, due to the fact that breakup is not included explicitly in the parametrization normally used to fit the optical potential. In this case, we take the effective deuteron absorption cross section to be 0 and adjust the reaction cross section accordingly. Since all of the cross sections are associated with absorption by the same target, the latter corrections are small, when they occur. These considerations are taken into account automatically in the modified version of the reaction code EMPIRE.

The differences between the partial wave contributions to the cross sections can be clearly seen when these are written in terms of the corresponding effective transmission coefficients $T_l$, defined as

$$\sigma_l = \frac{\pi}{k_d^2} (2l+1)\, T_l \,. \tag{10}$$

In Fig. 3, we show the effective transmission coefficients for the breakup and absorption processes of a 15 MeV deuteron incident on $^{238}$U. The solid line represents the total reaction cross section. Its value of about one for lower partial waves indicates that almost all flux in the internal region of the nucleus is removed from the elastic channel. The dashed-dotted and dashed-double-dotted lines correspond to the fraction of the flux that leads to proton or neutron absorption following a (nonelastic) breakup reaction in which the other particle is emitted. It is interesting to note that both processes have substantial contributions from the internal region. We also note that more protons are absorbed than neutrons. These are common features of all of our calculations. The deuteron absorption cross section, obtained by subtracting the breakup contributions from the reaction cross section, is shown by the dashed line in the figure. We note that it corresponds to little more than 60% of the absorbed flux in the nuclear interior, with the remainder of the reaction flux corresponding to the breakup channels. Finally, the contribution of elastic breakup, denoted by the dotted line in the figure, is small in the nuclear interior and possesses a small but long Coulomb tail, only partially shown in the figure. Elastic breakup does not form a compound nucleus, but contributes to the inclusive emission spectra. At much higher energies, we observe that the breakup channels dominate the reaction cross section in the nuclear surface, limiting deuteron absorption to the interior region.

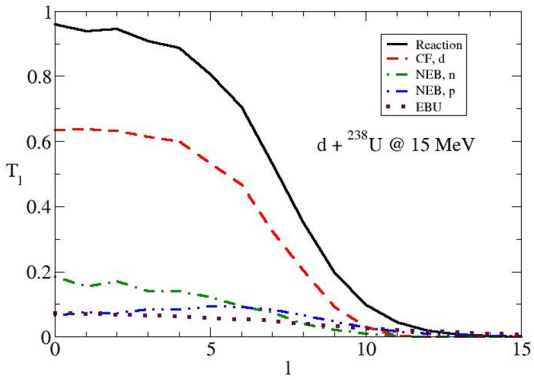


**Figure 3.** The partial wave contributions to the reaction cross section (solid black line), of deuteron absorption (dashed red line), proton (dashed-dotted green line) and neutron (dashed-double-dotted blue line) *absorption* from nonelastic breakup, and elastic breakup (dotted magenta line) are shown for deuterons incident at 15 MeV on $^{238}$U. More details can be found in the text.

## 3 The (d,2n) reaction

The (d,2n) reaction is of special interest for several reasons. Deuteron breakup reduces the two-step compound nucleus reaction cross section

d+(Z,A) → (Z+1,A+2)$^*$ → (Z+1,A+1)$^*$+n → (Z+1,A)+2n

because of the flux lost to breakup. Part of the flux returns, however, through the nonelastic (NEB, n) reaction,

d+(Z,A) → p+n+(Z,A) → (Z+1,A+1)$^*$+n → (Z+1,A)+2n.

For heavy nuclei, the Coulomb barrier inhibits charged particle emission so that neutron emission dominates. The compound nuclear emission cross section is then a function of the absorption cross sections (deuteron, proton and neutron) and the breakup one. As all of these cross sections are constrained by other emission channels as well, the (d,2n) reaction provides a test of the ability of the breakup-fusion model to describe details of the breakup process, such as its angular momentum and energy transfer, correctly. Our calculations for a number of target nuclei are shown below.

We find the overall agreement between the calculations and the experimental data to be good. We observe, however, a consistent overestimation of the data at higher incident energies. We believe this to be due to issues with pre-equilibrium emission in the calculations. Although we take into account pre-equilibrium emission after deuteron absorption, it is not taken into account in proton absorption after a breakup reaction. With increasing energy, the

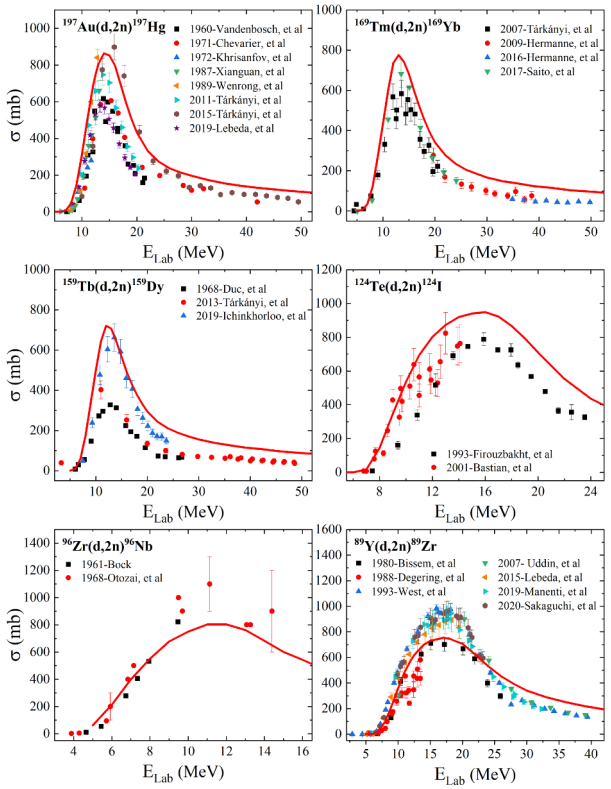


**Figure 4.** Theoretical cross sections, represented by solid curves, are compared with experimental data for various (d,2n) reactions, including $^{197}$Au(d,2n)$^{197}$Hg [20–27], $^{169}$Tm(d,2n)$^{169}$Yb [28–31], $^{159}$Tb(d,2n)$^{159}$Dy [32–34], $^{124}$Te(d,2n)$^{124}$I [35, 36], $^{96}$Zr(d,2n)$^{96}$Nb [37, 38], and $^{89}$Y(d,2n)$^{89}$Zr [39–45].

breakup proton would have an increasing probability of being emitted before equilibrium is reached. Taking this reaction into account would reduce the cross section at these energies and provide better agreement with the data. Despite the general good agreement seen here, the examination if isomeric and ground states cross sections, not shown here, reveals large discrepancies between the experimental data and the calculations in several cases. Such disparities require further investigation before any firm conclusion can be reached.

Inelastic neutron scattering is known to be important for heavy deformed nuclei, such as most of those for which we have calculated (d,2n) cross sections. However, inelastic scattering is not taken into account in our calculations. If it were to be an important part of the nonelastic cross section, it would reduce the nonelastic flux available for formation of the compound nucleus. Alternatively, if the breakup process itself is inelastic, the energy available to the proton in a (NEB, n) reaction would be smaller on the average, thereby reducing its fusion probability and again reducing the formation of the compound nucleus. Since inelastic scattering increases with the deformation, we might expect to find a correlation between the deformation of a nucleus and any discrepancy between the experimental data and our calculations. We would expect the calculation, which does not take into account the effects of

**Table 1.** Quadrupole deformations $\beta_2$ for selected targets, extracted from mean field calculations using the DDME2 RMF [46], the FRDM [47] and a Sk-HFB model [48].

| Nucleus | DDME2 | FRDM | Sk-HFB |
|---|---|---|---|
| $^{197}$Au | -0.130 | -0.125 | -0.140 |
| $^{169}$Tm | 0.346 | 0.298 | 0.360 |
| $^{159}$Tb | 0.311 | 0.271 | 0.350 |
| $^{124}$Te | -0.135 | -0.125 | -0.140 |
| $^{93}$Nb | 0.123 | 0.011 | -0.110 |
| $^{96}$Zr | 0.254 | 0.240 | -0.220 |
| $^{89}$Y | 0.000 | 0.000 | 0.000 |

inelastic scattering, to overestimate the experimental data at low energies, where the inelastic scattering is most important. An examination of the calculations based on the mean filed deformations given in Table 1, reveals no such correlation. We thus conclude, tentatively, that inelastic scattering does not play an important role in the breakup-fusion reaction, although it could still play a role in direct emission from the breakup reaction, as we have seen in the double differential spectra of Figs. 1 and 2.

## 4 The (d,pf) reaction

At low excitation energies, charged particle emission from a heavy target is strongly inhibited. In a deuteron-induced reaction, the target + neutron nucleus will be populated almost exclusively in this case by breakup followed by neutron fusion and proton emission. Here, we compare model predictions with recent experimental data for the reaction $^{238}$U(d,pf). We assume that the (d,p) channel leads exclusively to elastic breakup or to nonelastic breakup with absorption of the neutron. To study the $^{239}$U fission induced by the absorbed neutron, we need a good description of the fission barriers and barrier densities, as the entrance channel properties of the breakup neutron are not the same as those of a normal incident neutron. Here we use fission barrier and barrier density parameters obtained from the recent CIELO evaluation of neutron-induced reactions on $^{238}$U [49]. The neutron-induced fission cross section, $^{238}$U(n,f), obtained using these parameters is compared to experimental data taken from the EXFOR library in Fig. 6. We note that the agreement is good but far from perfect, due to the fact that we did not take into account all of the nuances of the evaluation.

We show in Fig. 6 the calculated angular distributions of protons emitted after the breakup of deuterons incident on $^{238}$U at 15 MeV. The black solid curve corresponds to the inclusive elastic plus nonelastic (EBU + NEB, p) proton emission. The blue dashed curve corresponds to the protons emitted from breakup reactions in which the neutron was absorbed, the (NEB, p) reaction. At forward angles the elastic breakup dominates the angular distribution, while at backward angles the ratio between the two angular distributions is fairly constant and the curves run in parallel.

Two measurements of the (d,pf) reaction exist, on with 18 MeV deuterons, by Britt and Cramer in 1970 [51] and

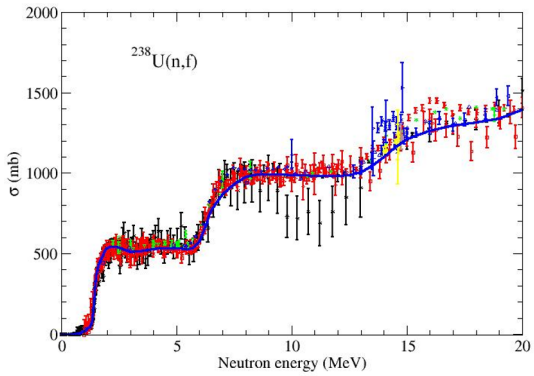


**Figure 5.** The $^{238}$U(n,f) fission cross section calculated with fission barrier and density parameters of the CIELO evaluation [49] (blue curve) compared to experimental data obtained from the EXFOR library [50].

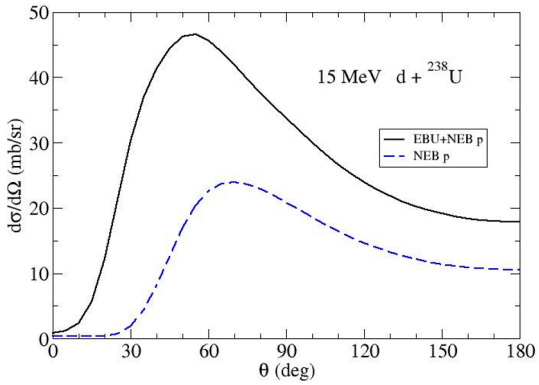


**Figure 6.** The nonelastic (NEB, p) proton emission and inclusive (EBU + NEB, p) proton emission angular distributions from deuterons incident on $^{238}$U at 15 MeV.

a more recent one with deuterons of 15 MeV by Ducasse et al. [52]. The more recent experimental measurement of the (d,pf) reaction was performed at two backward angles, 126° and 140°. The counts observed as a function of proton emission energy were converted to fission probabilities, $P_f$, as the ratio of coincidences of proton emission with fission $N(p \text{ and } f)$ divided by the total number of proton emissions $N(p)$ and the efficiency of fission detection $\varepsilon(f)$,

$$P_f = \frac{N(p \text{ and } f)}{N(p)\,\varepsilon(f)}.$$

The fission probabilities obtained at the two angles were very similar. The experimental group also measured the probability of gamma emission in coincidence with proton emission in a similar manner. In this case, they found the gamma emission probability to be about 50% higher at the smaller angle.

The experimental deuteron-induced $^{239}$U fission probability is the ratio of the coincident proton-fission cross section to the inclusive proton cross section, which contains a large contribution from the elastic breakup protons, where the neutrons are also emitted. Although this quantity can be calculated theoretically, a more meaningful definition of the fission probability would compare the coincidence count to the count of protons for which the neutron was absorbed, that is the (NEB, p) cross section. The differential spectra for elastic (EBU), nonelastic (NEB, p) and inclusive (EBU + NEB, p) proton emission from deuteron breakup on $^{238}$U at 15 MeV are shown in Fig.7 as a function of the equivalent excitation energy of the $^{239}$U nucleus. The nonelastic proton emission (NEB, p) dominates at low excitation energy but is surpassed by the elastic breakup at higher energies. To convert the experimental data to a more meaningful fission probability, the data should be rescaled by the ratio of the inclusive proton emission spectrum over the nonelastic (NEB, p) one.

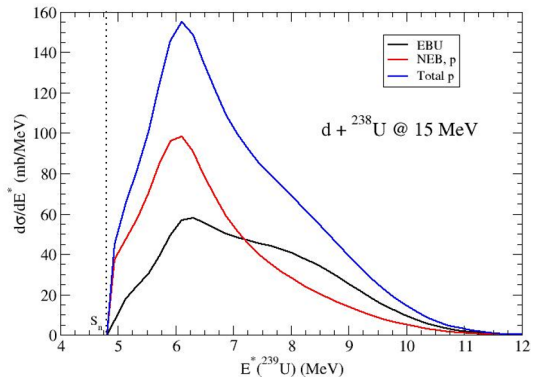


**Figure 7.** The differential spectra for elastic (EBU), nonelastic (NEB, p) and inclusive (EBU + NEB, p) proton emission from deuteron breakup on $^{238}$U at 15 MeV.

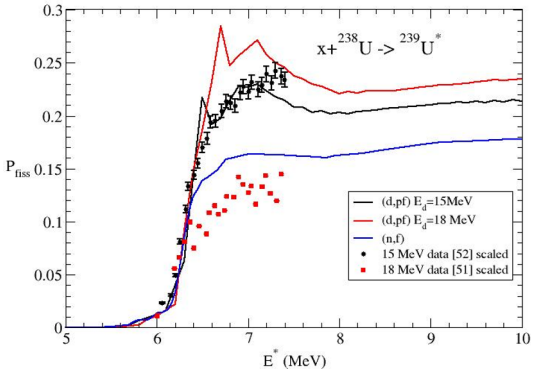


**Figure 8.** The $^{238}$U(n,f) and $^{238}$U(d,pf) fission probabilities calculated with EMPIRE are compared to the rescaled experimental data of Refs. [51] and [52].

In Fig.8, we compare the rescaled experimental fission data with fission probabilities for $^{238}$U(n,f) and $^{238}$U(d,pf) calculated with EMPIRE using the optical potentials and fission barriers and densities of the CIELO evaluation [49]. We observe that the deuteron fission probability exceeds the neutron one by a factor of 30% to 50%. This is an effect of the greater angular momentum transferred by the neutron of the deuteron at an energy equivalent to that for a solitary neutron. We observe that the corrected data of Britt and Cramer [51] is still about a factor of two lower than expected theoretically, but that the data of Ducasse et

al. [52] is reasonably well described by the model. Although we have no explanation for the great difference between the Britt and Cramer data and the calculation, the agreement with the Ducasse et al. data is quite encouraging.

## 5 Conclusions

This study is devoted to an analysis of the ability of an extended theoretical framework consisting of the IAV breakup model coupled to pre-equilibrium and equilibrium compound nuclear emission to describe inclusive nucleon emission spectra as well as compound nuclear production cross sections in deuteron-induced reactions. To this end, the IAV breakup model has been integrated in the nuclear reaction code for the specific case of deuteron-induced reactions. The results obtained are quite promising. The extended model furnishes a generally good description of the inclusive differential and total emission cross sections for both protons and neutrons. We also obtain very reasonable results for the total (d,2n) activation cross section over a wide range of energies, as well as encouraging results for the fission probability of the exclusive $^{238}$U(d,pf) reaction.

There is still much room for improvement, however. The calculated inclusive differential emission spectra tend to lie at slightly higher energy than the experimental ones, suggesting energy loss associated with inelastic scattering. The theoretical calculations also systematically underestimate the magnitude of the forward angle breakup cross section of deuterons incident on heavier targets. The theoretical (d,2n) activation cross sections systematically overestimate the experimental ones at high energy, which suggest that pre-equilibrium proton emission is underestimated in the calculations. Calculations of the exclusive $^{238}$U(d,pf) fission probability showed good agreement with one set of experimental data but poor agreement with another set. More precise calculations as well as more data are needed.

Finally, we note that the deuteron is the simplest nucleus susceptible to breakup. Many other light projectiles possess fragments with excited states or more complex three or four body breakup modes. Even the next simplest cases, $^{3}$H and $^{3}$He, possess both two- and three-body breakup modes. The IAV model provides a reasonable description of the two-body breakup channel in these cases [53], but no attempt has yet been made to describe the three-body breakup modes. There is clearly much to be done.

## Acknowledgement

BVC and FT acknowledge the support of grants 2017/05660-0 and 2020/04160-6 of the São Paulo Research Foundation (FAPESP), grant 303131/2021-7 of the CNPq, and the INCT-FNA project 464898/2014-5. BVC also acknowledges support from the NAPC-Nuclear Data Section of the IAEA.

## References

[1] N. Austern and C. M. Vincent, Phys. Rev. C **23**, 1847 (1981). https://doi.org/10.1103/PhysRevC.23.1847
[2] A. Kasano and M. Ichimura, Phys. Lett. B **115**, 81 (1982). https://doi.org/10.1016/0370-2693(82)90800-0
[3] N. Austern, Y. Iseri, M. Kamimura, M. Kawai, G. Rawitscher, and M. Yahiro, Phys. Rep. **154**, 125 (1987). https://doi.org/10.1016/0370-1573(87)90094-9
[4] M. Ichimura, Phys. Rev. C **41**, 834 (1990). https://doi.org/10.1103/PhysRevC.41.834
[5] Jin Lei and A. M. Moro, Phys. Rev. C **92**, 044616 (2015); 061602(R) (2015). https://doi.org/10.1103/PhysRevC.92.044616
[6] B. V. Carlson, R. Capote and M. Sin, Few-Body Systems **57**, 307 (2016). 10.1007/s00601-016-1054-8
[7] G. Potel et al., Eur. Phys. J. A **53**, 178 (2017). https://doi.org/10.1140/epja/i2017-12371-9
[8] F. Torabi and B. V. Carlson, J. Phys. G **50**, 045107 (2023). 10.1088/1361-6471/acb95f
[9] M. Herman, R. Capote, B. V. Carlson, P. Oblozinský, M. Sin, A. Trkov, H. Wienke, V. Zerkin, Nucl. Data Sheets **108**, 2655 (2007). https://doi.org/10.1016/j.nds.2007.11.003
[10] P. J. A. Buttle and L. J. B. Goldfarb, Proc. Phys. Soc. (London) **83**, 701 (1964).
[11] G. Bencze and J. Zimanyi, Phys. Lett. **9**, 246 (1964).
[12] C. M. Vincent and H. T. Fortune, Phys. Rev. C **2**, 782 (1970). https://doi.org/10.1103/PhysRevC.2.782
[13] A. Sommerfeld, Atombau und Spektrallinien, Bd.2 (Vieweg, Braunschweig, 1939).
[14] L. Landau and E. Lifschitz, JETP **18**, 750 (1948).
[15] A. Nordsieck, Phys. Rev. **93**, 785 (1954). https://doi.org/10.1103/PhysRev.93.785
[16] A. J. Koning and J. P. Delaroche, Nucl. Phys. A **713**, 231 (2003). https://doi.org/10.1016/S0375-9474(02)01321-0
[17] H. An and C. Cai, Phys. Rev. C **73**, 054605 (2006). https://doi.org/10.1103/PhysRevC.73.054605
[18] N. Matsuoka et al., Nucl. Phys. **A345**, 1 (1980). 10.1016/0375-9474(80)90409-1
[19] S. Araki et al., Nucl. Instrum. Methods Phys. Res. A **842**, 62 (2017). https://doi.org/10.1016/j.nima.2016.10.043
[20] R. Vandenbosch and J. R. Huizenga, Phys. Rev. **120**, 1313 (1960). https://doi.org/10.1103/PhysRev.120.1313
[21] N. Chevarier, A. Chevarier, A. Demeyer, and T. M. Duc, Journal de Physique, **32**, 483 (1971). 10.1051/jphys:01971003207048300
[22] Yu. V. Khrisanfov,V. Yu. Padalko,P. P. Zarubin, Izv. Rossiiskoi Akademii Nauk, Ser.Fiz. **36**, 641 (1972).
[23] Long Xianguan, Peng Xiufeng, and He Fuqing, Chinese J.of Nuclear Physics (Beijing) **9**, 48 (1987).
[24] Zhao Wenrong, and Lu Hanlin, Chinese J.of Nuclear Physics (Beijing) **11**, 83 (1989).
[25] F. Tárkányi, F. Ditrói, A. Hermanne, S. Takács, B. Király, H. Yamazaki, M. Baba, A. Mohammadi, and A.V. Ignatyuk, Nucl. Instrum. Methods Phys. Res. B **269**, 1389 (2011).

https://doi.org/10.1016/j.nimb.2011.03.019

[26] F. Tárkányi, A. Hermanne, F. Ditrói, S. Takács, R. Adam Rebeles, and A. V. Ignatyuk, Nucl. Instrum. Methods in Phys. Res. B **362**, 116 (2015). https://doi.org/10.1016/j.nimb.2015.09.044

[27] O. Lebeda and J. Červenák, Nucl. Instrum. Methods Phys. Res. B, **461**, 105 (2019). https://doi.org/10.1016/j.nimb.2019.09.034

[28] F. Tárkányi, A. Hermanne, S. Takács, F. Ditrói, I. Spahn, S. F. Kovalev, A. V. Ignatyuk, and S. M. Qaim, Appl. Radiat. Isot. **65**, 663 (2007). https://doi.org/10.1016/j.apradiso.2007.01.008

[29] A. Hermanne, F. Tárkányi, S. Takács, F. Ditrói, M. Baba, T. Ohtshuki, I. Spahn, and A. V. Ignatyuk, Nucl. Instrum. Methods Phys. Res. B **267**, 727 (2009). 10.1016/j.nimb.2008.12.017

[30] A. Hermanne, F. Tárkányi, S. Takács, and F. Ditrói, Nucl. Instrum. Methods Phys. Res. B **383**, 81 (2016). https://doi.org/10.1016/j.nimb.2016.06.010

[31] M. Saito, M. Aikawa, Y. Komori, H. Haba, and S. Takács, Appl. Radiat. Isot. **125**, 23 (2017). 10.1016/j.apradiso.2017.04.010

[32] MM. T. M. Duc, J. Tousset, and M. F. Perrin, Comptes rendus hebdomadaires des séances de l'Académie des sciences, Série B, Physique, **266**, 100 (1968).

[33] F. Tárkányi, S. Takács, F. Ditrói, A. Hermanne, and A. V. Ignatyuk, Nucl. Instrum. Methods Phys. Res. B **316**, 183 (2013). https://doi.org/10.1016/j.nimb.2013.09.008

[34] D. Ichinkhorloo, M. Aikawa, T. Zolbadral, Y. Komori, and H. Haba, Nucl. Instrum. Methods Phys. Res. B **461**, 102 (2019). https://doi.org/10.1016/j.nimb.2019.09.037

[35] M. L. Firouzbakht, D.J. Schlyer, R.D. Finn, G. Languzzi,A.P. Wolf, Nucl. Instrum. Meth. B **79**, 909 (1993). https://doi.org/10.1016/0168-583X(93)95496-R

[36] T. Bastian, H.H. Coenen, S.M. Qaim, Appl. Radiat. Isot. **55**, 303 (2001). https://doi.org/10.1016/S0969-8043(01)00079-3

[37] R. Bock, Zeitschrift fuer Physik, **164**, 546 (1961). 10.1007/BF01378428

[38] K. Otozai, S. Kuze, H. Okamura, A. Mito, T. Nishi, and I. Fujiwara, Nucl. Phys. A **107**, 427 (1968). https://doi.org/10.1016/0375-9474(68)90630-1

[39] H. H. Bissem, R. Georgi, W. Scobel, J. Ernst, M. Kaba, J. Rama Rao, and H. Strohe, Phys. Rev. C **22**, 1468 (1980). https://doi.org/10.1103/PhysRevC.22.1468

[40] D. Degering, S. Unterricker, W. Stolz, J. Radioanal. Nucl. Chem. Lett. **127**, 7 (1988).https://doi.org/10.1007/BF02165500

[41] H. I. West, H. O. Brien, R. G. Lanier, R. J. Nagle, and M. G. Mustafa, Prog: U.C., Lawrence Rad.Lab. (Berkeley and Livermore) **4**, 115738-1 (1993).

[42] M. S. Uddin, M. Baba, M. Hagiwara, F. Tárkányi, and F. Ditrói, Radiochimica Acta, **95**, 187 (2007). https://doi.org/10.1524/ract.2007.95.4.187

[43] O. Lebeda, J. Štursa, and J. Ráliš, Nucl. Instrum. Methods Phys. Res. B **360**, 118 (2015). https://doi.org/10.1016/j.nimb.2015.08.036

[44] S. Manenti, F. Haddad, and F. Groppi, Nucl. Instrum. Methods Phys. Res. B **458**, 57 (2019). https://doi.org/10.1016/j.nimb.2019.08.002

[45] M. Sakaguchi, M. Aikawa, M. Saito, N. Ukon, Y. Komori, and H. Haba, Nucl. Instrum. Methods Phys. Res. B **472**, 59 (2020). https://doi.org/10.1016/j.nimb.2020.04.003

[46] L. C. Chamon, B. V. Carlson, and L. R. Gasques, Comp. Phys. Comm. **267**, 108061 (2021). https://doi.org/10.1016/j.cpc.2021.108061

[47] P. Möller, A. J. Sierk, T. Ichikawa, and H. Sagawa, At. Data Nucl. Data Tables **109–110**, 1 (2016). https://doi.org/10.1016/j.adt.2015.10.002

[48] S. Goriely, M. Samyn, P.-H. Heenen, J. M. Pearson, and F. Tondeur, Phys. Rev. C **66**, 024326 (2002). https://doi.org/10.1103/PhysRevC.66.024326

[49] R. Capote et al., Nucl. Data Sheets **148**, 254 (2018). https://doi.org/10.1016/j.nds.2018.02.005

[50] Experimental Nuclear Reaction Data (EXFOR) Database. https://www-nds.iaea.org/exfor/

[51] H.C. Britt and J.D. Cramer, Phys. Rev. C **2**, 1758 (1970). https://doi.org/10.1103/PhysRevC.2.1758

[52] Q. Ducasse et al., Phys. Rev. C **94**, 024614, (2016). https://doi.org/10.1103/PhysRevC.94.024614

[53] E. V. Chimanski, L. A. Souza and B. V. Carlson, Braz. J. Phys. **51**, 323 (2021). https://doi.org/10.1007/s13538-020-00819-x